



Ground-based hyperspectral measurement at visible-infrared wavelengths for validation of the atmospheric carbon dioxide absorption wavebands in the context of AVIRIS-NG flight over Kolkata-Howrah

Barun Raychaudhuri¹ and Sasmita Chaurasia²

¹Department of Physics, Presidency University, 86/1 College Street, Kolkata 700073

²Space Applications Centre (SAC), ISRO, Ahmedabad, 380015

Email: barun.physics@presiuniv.ac.in; sasmita@sac.isro.gov.in

(Received: Aug 08, 2017; in final form: Sep 27, 2017)

Abstract: The paper validates the atmospheric absorption of solar radiation due to carbon dioxide (CO₂) by comparing the average wavelengths of maximum absorption obtained from ground-based spectroradiometric measurement with those derived from the hyperspectral image of Next Generation Airborne Visible Infrared Spectrometer (AVIRIS-NG) procured by SAC-ISRO and that of Hyperion downloaded from USGS website for urban areas of Kolkata, India. The field spectrometry of atmospheric irradiance was carried out at 1 nm resolution of spectral data over the range of 400-2400 nm with ASD spectroradiometer fitted with remote cosine receptor. The effects of the changes in CO₂ concentration due to change of altitude, airmass and urban congestion were reflected on the measured spectra. The spectral radiance over the same wavelength range derived from the airborne and the space-borne image were of 5 and 10 nm resolution, respectively. The CO₂ absorption wavelengths detected at around 2 μm from AVIRIS-NG and Hyperion images were found to deviate by less than 1% from that obtained from the ground data.

Keywords: Hyperspectral, CO₂, AVIRIS-NG.

1. Introduction

Carbon dioxide (CO₂), the most remarkable anthropogenic greenhouse gas has enhanced its existence in the atmosphere from a pre-industrial average level of 280 ppm to more than 388 ppm as of June 2010 (Boesch et al., 2011). The main reasons are human activities, such as burning of fossil fuel and change of land use. Therefore, the global monitoring of CO₂ abundance has been realized as an event of prime importance (Etheridge et al., 1996; Bousquet et al., 2000; Canadell et al., 2007). In order to develop worldwide effort of controlling the CO₂ emission, accurate monitoring systems have been set up for CO₂ production and sinking through ground-based (Wunch et al., 2011; Buschmann et al., 2016), airborne (Gao et al., 2009; Tadic et al., 2014; Tanaka et al., 2016) and satellite-based (Bovensmann et al., 1999; Hamazaki et al., 2004; Boesch et al., 2011; Crisp et al., 2012; Kuze et al., 2014; Wei et al., 2014; Watanabe et al., 2015; Frankenberg et al., 2015) observations.

The significance of field-based hyperspectral CO₂ monitoring may be realized as a validation system for the airborne and satellite-borne hyperspectral sensors and also as a primary step toward establishing ground-based CO₂ monitoring network similar to Total Carbon Column Observing Network (TCCON) (Wunch et al., 2011) and others (Buschmann et al.,

2016) that can provide accurate local data and identify the different reasons, such as human activities, burning of fossil fuel and running vehicles and industries for enhancing the atmospheric abundance of CO₂ in high precision. Installation of such ground-based carbon observation system in tropical countries like India is recommended in recent work (Raychaudhuri, 2017). This work analyses a field survey on atmospheric irradiance measurement with spectroradiometer at around 1 nm of spectral resolution. It detects the radiation absorption due to atmospheric gases closer to the actual physical phenomenon of sub-nanometer level change whereas the airborne or satellite-based measurements yield only a gross average over 5-10 nm. However, the later ones alone are the practical techniques for observation over large areas. Considering these, the present work intends to standardize the wavelengths of carbon dioxide absorptions retrieved from the hyperspectral images and its extent of deviation from the actual ground condition. It validates the absorption wavebands for CO₂ on the spectral reflectance of solar radiation by comparing the ground spectra with that derived from recently procured AVIRIS-NG images of Kolkata, India and Hyperion images for similar regions. This is actually based on a pilot work (Raychaudhuri and Chaurasia, 2017) that has conceived ideas on assessing the atmospheric CO₂ content and its spatial variation for further studies.

2. Materials and method

The work contains data procurement from both field spectrometry and airborne sensor data analysis, as follows.

2.1 Image analysis

For the first time, Space Applications Centre, Indian Space Research Organization (SAC, ISRO) conducted flight of the airborne hyperspectral optical sensor named Next Generation Airborne Visible Infrared Spectrometer (AVIRIS-NG) in 2016 over India and procured hyperspectral images over ultraviolet-visible-near-infrared-shortwave-infrared wavelength ranges for different sites as indicated in Figure 1.

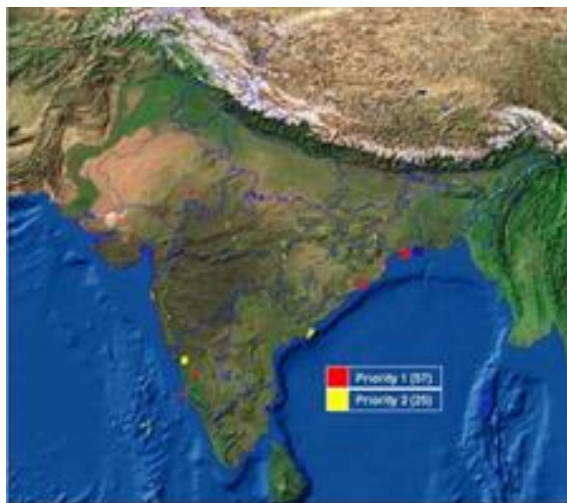


Figure 1: AVIRIS-NG science campaign site over India

The AVIRIS-NG campaign over selected areas of two adjacent cities, namely Howrah and Kolkata was executed between February 24 and March 06, 2016. Figure 2 shows a part of the densely populated areas of Howrah and Kolkata accommodated to the AVIRIS-NG image. The regions 'A' and 'B' denote two densely populated areas of Howrah and Kolkata, respectively. The zone marked as 'Vg' corresponds to the vegetated area and the region 'C' points out water body. It is actually part of river Hooghly. Since the images were available for some portions of urban areas of Kolkata city (around $22^{\circ} 32' 30''$ N, $88^{\circ} 19' 30''$ E), the ground-based spectroradiometric data were collected at different urban places of Kolkata at almost the same season (spring) of AVIRIS-NG image procurement. Two Hyperion images downloaded from USGS website were also used, which comprised the regions nearby our study region. Spectral reflectance values were derived from the images. The radiance



Figure 2: Part of Howrah and Kolkata as captured by AVIRIS-NG image

curves for AVIRIS-NG were readily available because the images were pre-processed for stack layering. The Hyperion image layers were stacked using ENVI 4.7 image processing software and the DN values were converted to reflectance following conventional technique (Griffin et al., 2005).

2.2 Ground-based hyperspectral measurement

The incident solar irradiance was measured with Analytical Spectral Devices (ASD) FieldSpec spectroradiometer at high spectral resolution (1 nm) throughout the ultraviolet-visible-near-infrared and shortwave infrared wavelengths. The ASD FieldSpec spectroradiometer has sampling interval of 1.4 nm for the wavelength range of 350 - 1000 nm and that of 2 nm for the range of 1000 - 2500 nm. It has Full Width at Half Maximum (FWHM) spectral resolution of 3 nm and 10 nm for the wavelength ranges of 350 -1000 nm and 1000 - 2500 nm, respectively. Interpolating the above wavelength-channels it produces data points of 1 nm resolution over the wavelength range of 350 – 2500 nm. The range of 400–2400 nm is reported here. All the measurements were carried out in open air under cloud-free solar illumination. In order to integrate the incident solar radiation for both direct and diffused components, the measurements were executed by fitting a remote cosine receptor on the 25 degree field-of-view fibre. The instrument was kept vertically sky-facing with the help of the attached spirit level irrespective of the solar elevation. Data were collected for two consecutive days at different places of the urban area of varying population and

altitude. Variation of solar elevation, illumination and the time of the day were included in the measurement. Table 1 summarizes the type of the measurement sites and the modes of data collection. Table 2 compiles the data procured at a single site (Site 1) throughout the morning up to solar noon so as to correspond to the change in solar elevation. Along with the spectral measurements, the atmospheric CO₂ concentrations

(in ppm) at the ground surface were measured simultaneously with handheld carbon dioxide meter Model GCH-2018 at each site. It provided ancillary data for developing some model for the possible vertical profiles of CO₂ concentration and spatio-temporal variation. The solar illumination corresponding to each irradiance recording was measured with Metravi light intensity meter.

Table 1: Solar irradiance measurement with ASD spectroradiometer and CO₂ concentration for different sites over Kolkata

Site No.	Ambient condition	Approx. Time	CO ₂ conc. at the spot (ppm)	Solar illumination (klux)
1	Less population and vehicle	9 AM	410	48-49.2
		10.30 AM	386	58-63
2	Densely populated, busy road	11:30 to 11:45 AM	540	67.2
3	Grass field	11:45 to 12 noon	404	61.1
4	Car park	12 to 12:10 PM	504	58-58.2
5	Grass field of another zone	1:15 to 1:30 PM	450-453	62.5
6	7 th floor rooftop, windy atmosphere	1:30 to 1:45 PM	370-395	55-57.2

Table 2: Solar irradiance measurement with ASD spectroradiometer at site 1 at different times of morning

Approx. Time	CO ₂ conc. at the spot (ppm)	Solar illumination (klux)
7:00 AM	381	7.38-7.42
7:10 AM	392	6.9-7.02
7:30 AM	383-391	7.59-7.62
8:00 AM	383	14.02-14.28
8:05 AM	397-399	13.02-12.89
8:35 AM	394-395	16.0-16.23
9:10 AM	393-395	29-29.5
9:50 AM	387-388	53-54
9:52 AM	383-388	53-54
10:30 AM	390-392	61.6-61.9
11:00 AM	391-399	60.8-63.2
11:20 AM	363-365	60.4-61.3

3. Results and discussion

The radiation absorption by atmospheric gases is a molecular vibration phenomenon that involves sub-nanometer resolution of absorption spectrum. The

ground-based spectroradiometer detects it by averaging over 1 nm whereas the AVIRIS and Hyperion sensors do the same over 5 nm and 10 nm, respectively. Obviously the first one is closest to the actual physical process and free from the effect of surface reflectance. Considering the ground-based measurement of absorption through the atmospheric column as the standard one, the AVIRIS-NG data are compared with it.

The atmospheric irradiance spectra over the visible-infrared range of wavelength for sites 1, 4 and 6, as measured with ASD spectroradiometer are shown in Figure 3. The wavelength is expressed in micrometer in order to make the scale similar to that of AVIRIS-NG images. The CO₂ absorption is noted at around 2 μm on the spectral curve, as denoted in the figure. It is in good agreement in terms of absorption wavebands with the radiance spectrum obtained from AVIRIS-NG image (thick line and marked as 'Av') over the same wavelength range of 0.4 to 2.4 μm depicted in Figure 4 compared with similar radiance spectra obtained from Hyperion images marked as H1 (for July 2002) and H2 (for January 2010), respectively. Figure 5 and Figure 6 display the magnified views of the O₂-A and CO₂ absorptions on the spectral curves obtained from AVIRIS-NG (Figure 4) and spectroradiometer (Figure 3), respectively.

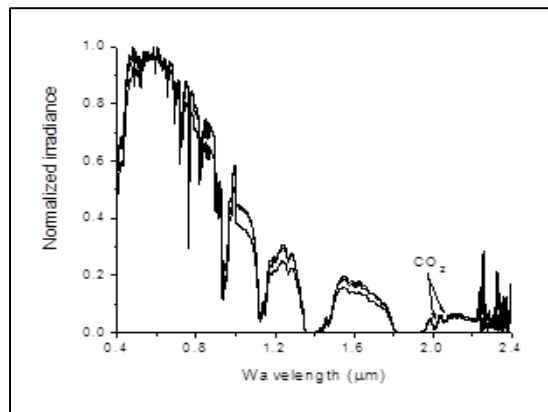


Figure 3: Atmospheric irradiance measured with ASD spectroradiometer plotted against wavelength. CO_2 absorption at around $2 \mu\text{m}$ is indicated against the curves

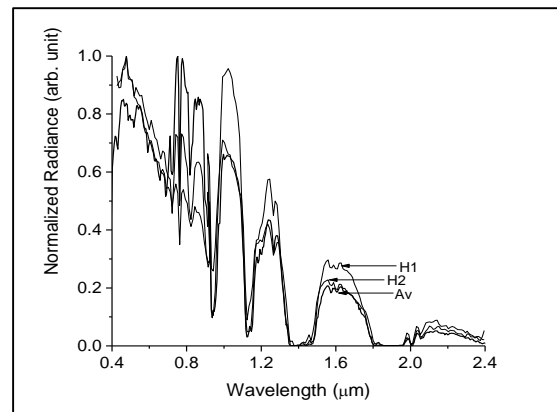


Figure 4: Radiance spectrum derived from AVIRIS-NG image of densely populated urban regions (thick line and marked as 'Av') compared with similar radiance spectra obtained from Hyperion images (marked as H1 and H2, respectively). CO_2 absorption is noted at around $2 \mu\text{m}$

Table 3: Comparison of the absorption maxima for atmospheric oxygen ($\text{O}_2\text{-A}$) and carbon dioxide ($\text{CO}_2\text{-1}$ and $\text{CO}_2\text{-2}$) obtained from ground-, air- and space-based data

Date Source	Sensor altitude in km	Wavelength (μm) for absorption maximum			Deviation (%) from ground-based result
		$\text{O}_2\text{-A}$	$\text{CO}_2\text{-1}$	$\text{CO}_2\text{-2}$	
ASD spectro radiometer	0 – 0.023	0.761	2.003- 2.006	2.053- 2.057	0
AVIRIS-NG	6 – 7	0.762 (band centre of $\pm 0.005 \mu\text{m}$)	2.004	2.054	0.3 – 0.8
Hyperion H1 monsoon season	705	0.762 (band centre of $\pm 0.01 \mu\text{m}$)	2.002	2.052	0.6 – 0.7
Hyperion H2 winter season	705	0.762 (band centre of $\pm 0.01 \mu\text{m}$)	2.002	2.052	0.6 – 0.7

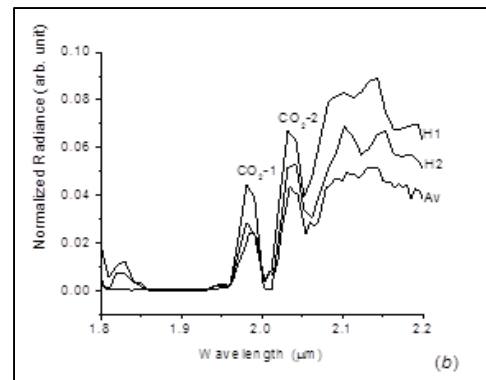
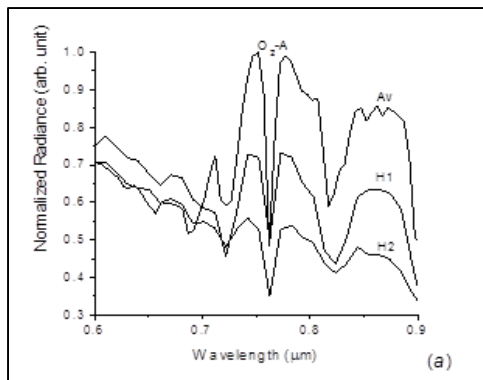


Figure 5: Expanded view of portions of the spectral curves of Fig. 4 to expose (a) the oxygen absorption ($\text{O}_2\text{-A}$) band; and (b) the carbon dioxide absorption ($\text{CO}_2\text{-1}$ and $\text{CO}_2\text{-2}$) bands

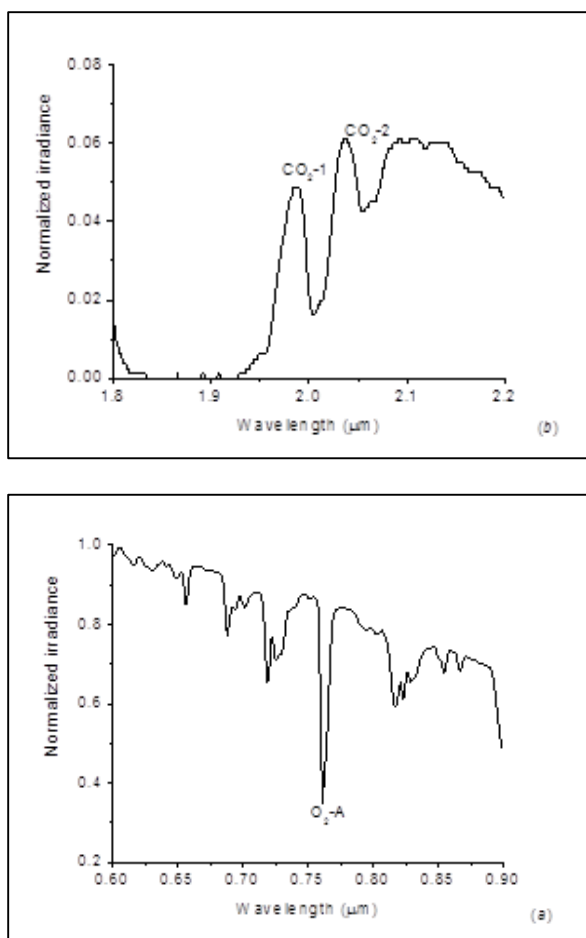


Figure 6: Expanded view of portions of the spectral curves of Fig. 3 to expose (a) the oxygen absorption (O₂-A) band and (b) the carbon dioxide absorption (CO₂-1 and CO₂-2) bands

A comparison of the wavelengths corresponding to O₂-A and CO₂ absorption maxima obtained from the above three sources is presented in Table 3. It quantifies the effects of sensor altitude and spectral resolution on the detection of absorption wavelength for atmospheric gases.

Irradiance observations at different locations indicate a wide variation of CO₂ due to population and automobile emission. It is observed from Table 1 that the CO₂ concentration at ground level at site 1, a suburban region, is around 400 ppm in comparison to more than 500 ppm at site 2 of dense population and vehicular emission. It is also observed that at ground level the CO₂ concentration (site 5) is nearly 450 ppm whereas that is 370-390 ppm at the roof top of a 7th floor building (site 6) at the same place, which indicates the vertical distribution of columnar CO₂ in the atmosphere. The variation of CO₂ at urban-

suburban region as well as at different elevation was picked up prominently in the ASD irradiance measurement as shown in Figure 7.

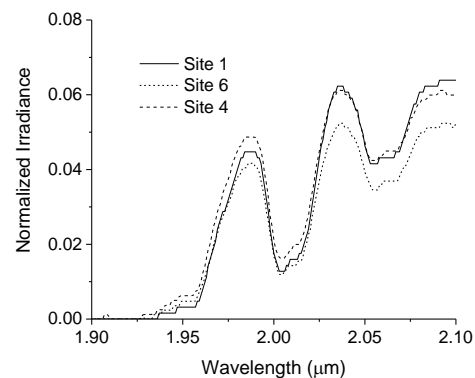


Figure 7: Variation of CO₂ absorption depth of spectroradiometric irradiance with its expected change in concentration with location and altitude

This work also investigates the change in absorption depth with solar elevation. The ground-level CO₂ concentration, as noted from Table-2, does not undergo any regular variation with solar elevation. It might be due to the fact that the local production of CO₂ at ground level due to vehicular emission or other reason masked the effect of solar elevation. Also the CO₂ absorption depth may not be strong enough to be detectable with weaker solar radiation, such as that in the early morning. Any way the effect of the change in solar elevation was not prominent in the CO₂ absorption on the spectral curves procured at different time (not shown). In such a condition, an alternative is suggested with oxygen (O₂-A) absorption, as indicated with Figure 8.

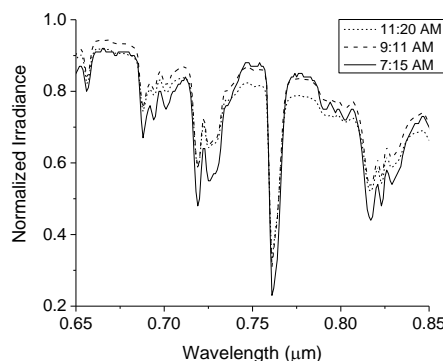


Figure 8: Variation of spectroradiometric O₂-A absorption depth with solar zenith angle at a particular location (site 1) for different time of the day

As is apparent from the figure, the strong O₂-A absorption depth decreases regularly with increase of solar elevation. The principle of differential optical absorption spectroscopy (DOAS) (Platt and Stutz 2008) is to estimate the extent of radiation absorption through a certain atmospheric gaseous species by comparing the radiance at the absorbed and non-absorbed wavelengths on the spectral curve itself. The same principle is applied here. Assuming the wavelengths 755 nm and 778 nm as non-absorbing wavelength on either side of 761 nm, the wavelength of maximum absorption in Fig. 8, the average O₂-A absorption depth is found to change through 32% during four hours. Since the CO₂-1 and CO₂-2 absorptions are part of the same spectral curve, these absorption depths may be assumed to undergo similar variation. The 'white' solar radiation containing all the wavelengths corresponding to O₂-A, CO₂-1 and CO₂-2 passes through the same airmass at a certain instant of time and the radiation component of each wavelength undergoes absorption up to a certain fraction; different for different wavelength. When two such measurements taken at different solar elevations are compared, the absorption ratios are effectively multiplied by some proportionality constant.

The above discussed absorption depths for atmospheric gases may be affected by surface reflectance in the case of image-derived spectra and radiation scattering due to atmospheric aerosols for both image-derived and spectroradiometric measurements. However, it is mentioned earlier that the absorption depth is estimated from the principle of DOAS making use of the ratio of the radiance values at the absorbed and non-absorbed wavelengths obtained from the spectral curve itself. Since the span of the wavelengths for comparison is very short (e.g. 0.04 μm for CO₂ and 0.024 μm for O₂-A), the effects of perturbations like surface reflectance and atmospheric aerosol are expected to remain almost constant over the short range of wavelength and to be cancelled out in the ratio.

ASD measurements record only atmospheric phenomena whereas AVIRIS-NG records ground reflectance also causing difference in reflectance for different pixels. Figure 8 shows that the variation of O₂-A absorption depth is quite uniform. Assuming oxygen concentration as one-fifth of that of air, the absorption depth ratio of CO₂ to that of O₂-A can be used for quantifying CO₂. The spatial distribution of CO₂ can be determined from the image by estimating the absorption depth at each pixel. The vertical distribution of atmospheric CO₂ is expected to be estimated with respect to its measured value at ground level.

5. Conclusion

The signature of CO₂ absorption is clearly detected in both ground based (ASD) and airborne (AVIRIS-NG) hyperspectral measurements. The effect of change in CO₂ concentration is reflected in the data, e.g. with height and urban congestion. This work opens the possibility of further work on standardization of the CO₂ absorption depths near 2 μm in terms of absorbing and non-absorbing wavebands and calibration with respect to O₂-A band around 762 nm.

Acknowledgement

The AVIRIS-NG images were obtained at the courtesy of Space Applications Centre, Indian Space Research Organization. The technical help and moral support received all the way from Dr Arundhati Misra, Group Director, AMHTDG/EPSC of Space Applications Centre is thankfully acknowledged. The activity was undertaken under the approved AVIRIS-AG AO project, which will be funded by ISRO.

References

- Boesch, H., D. Baker, B. Connor, D. Crisp and C. Miller (2011). Global characterization of CO₂ column retrievals from shortwave-infrared satellite observations of the Orbiting Carbon Observatory-2 mission. *Remote Sensing*, 3, 270-304. doi:10.3390/rs3020270.
- Bousquet, P., P. Peylin, P. Ciais, C. Le Quere, P. Friedlingstein and P.P. Tans (2000). Regional changes in carbon dioxide fluxes of land and oceans since 1980. *Science*, 290, 1342-1346. doi:10.1126/science.290.5495.1342.
- Buschmann, M., N.M. Deutscher, V. Sherlock, M. Palm, T. Warneke and J. Notholt (2016). Retrieval of xCO₂ from ground-based mid-infrared (NDACC) solar absorption spectra and comparison to TCCON. *Atmospheric Measurement Techniques*, 9, 577-585. doi:10.5194/amt-9-577-2016.
- Bovensmann, H., J.P. Burrows, M. Buchwitz, J. Frerick, S. Noel and V.V. Rozanov (1999). SCIAMACHY: Mission objectives and measurement modes. *Journal of the Atmospheric Sciences*, 56, 127-150. doi:10.1175/1520-0469(1999)056<0127:SMOAMM>2.0.CO;2.
- Canadell, J.G., C. Le Quere, M.R. Raupach, C.B. Field, E.T. Buitenhuis, P. Ciais, T.J. Conway, N.P. Gillett, R.A. Houghton and G. Marland (2007).

Contributions to accelerating atmospheric CO₂ growth from economic activity, carbon intensity, and efficiency of natural sinks. *Proceedings of the National Academy of Sciences*, 104(47), 18866-18870. doi:10.1073/pnas.0702737104.

Crisp, D. and 33 others (2012). The ACOS CO₂ retrieval algorithm – part II: Global xCO₂ data characterization. *Atmospheric Measurement Techniques*, 5, 687-707.

Etheridge, D.M., L.P. Steele, R.L. Langenfelds, R.J. Francey, J.-M. Barnola and V.I. Morgan (1996). Natural and anthropogenic changes in atmospheric CO₂ over the last 1000 years from air in Antarctic ice and firn. *Journal of Geophysical Research*, 101, 4115-4128. doi:10.1029/95JD03410.

Frankenberg, C., R. Pollock, R.A.M. Lee, R. Rosenberg, J.-F. Blavier, D. Crisp, C.W. O'Dell, G.B. Osterman, C. Roehl, P.O. Wennberg and D. Wunch (2015). The Orbiting Carbon Observatory (OCO-2): Spectrometer performance evaluation using pre-launch direct sun measurements. *Atmospheric Measurement Techniques*, 8, 301-313. doi:10.5194/amt-8-301-2015.

Gao, B.-C., M. J. Montes, C.O. Davis and A.F.H. Goetz (2009). Atmospheric correction algorithms for hyperspectral remote sensing data of land and ocean. *Remote Sensing of Environment*, 113, S17-S24. doi:10.1016/j.rse.2007.12.015.

Griffin, M.K., S.M. Hsu, H-h.K. Burke, S.M. Orloff and C.A. Upham (2005). Examples of EO-1 Hyperion data analysis. *Lincoln Laboratory Journal*, 15, 271-298.

Hamazaki, T., Y. Kaneko and A. Kuze (2004). Carbon dioxide monitoring from the GOSAT satellite. *Proceedings of XXth ISPRS Conference 3-5, Istanbul, Turkey*, July 12-13, 2004.

Kuze, A., T.E. Taylor, F. Kataoka, C.J. Bruegge, D. Crisp, M. Harada, M. Helmlinger (2014). Long-term vicarious calibration of GOSAT short-wave sensors: Techniques for error reduction and new estimates of radiometric degradation factors. *IEEE Transactions on Geoscience and Remote Sensing*, 52(7), 3991-4004. doi:10.1109/TGRS.2013.2278696.

Platt, U. and J. Stutz (2008). Differential Optical Absorption Spectroscopy: Principles and Applications. Springer-Verlag Berlin Heidelberg, 2008.

Raychaudhuri, B. (2017). Spatial distribution of atmospheric CO₂ absorption detected around 2 μm on the reflectance spectra derived from Hyperion images. *International Journal of Remote Sensing*, 38(11), 3415-3429.
<http://dx.doi.org/10.1080/01431161.2017.1295483>.

Raychaudhuri, B. and Sasmita Chaurasia (2017). Ground-based spectroradiometric measurement over Kolkata for calibrating atmospheric carbon dioxide absorption wavebands in the context of AVIRIS-NG flight. *Scientific Report: AVIRIS-NG/AO/PU/SR-01 (Space Applications centre, Ahmedabad, INDIA)*

Tadic, J.M., M. Loewenstein, C. Frankenberg, A. Butz, M. Roby, L.T. Iraci, E.L. Yates, W. Gore and A. Kuze (2014). A comparison of in situ aircraft measurements of carbon dioxide and methane to GOSAT data measured over railroad valley Playa, Nevada, USA. *IEEE Transactions on Geoscience and Remote Sensing*, 52, 7764-7774. doi:10.1109/TGRS.2014.2318201.

Tanaka, T., E. Yates, L.T. Iraci, M.S. Johnson, W. Gore, J.M. Tadic and M. Loewenstein (2016). Two-year comparison of airborne measurements of CO₂ and CH₄ with GOSAT at railroad valley, Nevada. *IEEE Transactions on Geoscience and Remote Sensing*, 54, 4367-4375. doi:10.1109/TGRS.2016.2539973.

Watanabe, H., K. Hayashi, T. Saeki, S. Maksyutov, I. Nasuno, Y. Shimono, Y. Hirose, K. Takaichi, S. Kanekon, M. Ajiro, Y. Matsumoto and T. Yokota (2015). Global mapping of greenhouse gases retrieved from GOSAT level 2 products by using a kriging method. *International Journal of Remote Sensing*, 36, 1509-1528. doi:10.1080/01431161.2015.1011792.

Wei, J., A. Savtchenko, B. Vollmer, T. Hearty, A. Albayrak, D. Crisp and A. Eldering (2014). Advances in CO₂ observations from AIRS and ACOS. *IEEE Geoscience and Remote Sensing Letters*, 11, 891-895. doi:10.1109/LGRS.2013.2281147.